Exploratory habitation vehicles with trim intrinsic control

Meccanica
https://doi.org/10.1007/s11012-024-01839-6

RESEARCH

Exploratory habitation vehicles with trim intrinsic control

Andrea Manuello · Amedeo Manuello · Giuseppe Carlo Marano

Received: 24 April 2024 / Accepted: 9 June 2024

Abstract Considering the space environment and its critical issues and consequent risks, the challenge is to define the way and tools with which future astronauts will be able to act, live and work in space and, in particular on the Moon and Mars, exploiting, at the state of art, knowledge of innovative science, engineering and technology. On the Moon and Mars, the most obvious environmental factors are extreme temperature fluctuations, low gravity and the virtual absence of atmosphere and magnetosphere. The health of a human body can be damaged by reduced values of gravity. Due to the reduced gravity on the Moon and Mars, human bones and muscles are unloaded and begin to weaken. It increases the risk of bone fractures and atrophied muscles for astronauts returning to Earth from prolonged missions. The magnetosphere and atmosphere on Earth shield from much of the dangerous solar and cosmic radiation. Radiation with extremely high energies can damage even living tissue. The surface of the Moon and Mars has been crushed by millions of impacts of celestial bodies such as asteroids, leaving a layer of regolith that could be very deep depending on the areas of the planets. The habitation module, described in this paper, is carried by a vehicle equipped with two pairs of compass shaped legs that act as supports for the habitation module capable of maintaining a certain controlled height with respect to the ground as well as a horizontal attitude, during the movement of the compass. A system of ropes wound on pulleys allows to control the height of the habitat with respect to the ground, control the structure in movement, descent and ascent. The habitat can also be lowered to the ground. The geometry of the shape of the pulleys, around which the ropes are wound, is determined in such a way that the habitation module remains at a certain height during the movement defined by the two compass-shaped advancement supports. The paper describes and analyzes the movement of the pulleys during the entire phase of the movement of the habitation module and their geometric shape is discussed.

Keywords Space architecture · Space vehicle · Pulley system · Space habitat design

A. Manuello (✉)
Department of Mechanical and Aerospace Engineering, Politecnico di Torino, Corso Duca degli Abruzzi, 24, 10129 Turin, Italy
e-mail: andrea.manuello@polito.it

A. Manuello · G. C. Marano
Department of Structural, Geotechnical and Building Engineering, Politecnico di Torino, Corso Duca degli Abruzzi, 24, 10129 Turin, Italy

1 Introduction

Exploration and Colonization was always a big interest in human history, offering cultural, scientific, economic implications which involve many scientific and

Published online: 19 June 2024

technological needs including the design and realization creation of living habitation modules on extra-terrestrial soil, new types of spaceships and vehicles for exploration. This research and activities, related to space exploration, has also generated important spin-offs of inventions, technologies, and systems in response to the needs of daily life on earth [1, 2].

Among the objectives of space exploration is the colonization of the planets closest to Earth such as, firstly, the Moon and Mars. To colonize these planets, unmanned missions were carried out in the last century and, subsequently, manned missions were carried out on the Moon and are planned for Mars. This activity involves sheltered habitat, isolated from the spatial environment and systems to support the life of crew and guests. Moon and Mars are the closest targets for space exploration. The habitat vehicle described in this paper is aimed at these environments.

Using cutting-edge science, engineering, and technology to comprehend the lunar environment and its dangers, the challenge is to design and implement a plan for how future astronauts would live and operate on the Moon. The most noticeable environmental elements on the Moon are the pronounced temperature swings, the lack of an atmosphere, and the low gravity. The lunar surface is either very hot or extremely cold since there is no atmosphere to moderate the temperature variations. The average temperature ranges from 380 K in areas with sunlight to 30 K in areas without it. Extreme temperatures call for the necessity for suits and shelters.

The gravitational pull of the Moon is around 0.16 of that of Earth and that of the Mars is 0,38. There will be less weight on buildings and structures than there is on Earth. The human body may be negatively impacted by the decreased gravity. Because of the reduced gravity, human bones and strong muscles become unnecessary and start to weaken. This increases the danger of broken bones and weak muscles for astronauts returning to Earth. The magnetosphere and atmosphere of Earth shield the planet from a large portion of the hazardous solar and cosmic radiation. Radiation with extremely high energies can harm DNA and living tissue.

There is no atmosphere or magnetosphere on the Moon and On Mars the atmosphere is mainly composed of carbon dioxide and is much less dense than on Earth while the magnetosphere is almost absent. The surface of the ground has been crushed by millions of asteroid and comet impacts, leaving behind a layer of regolith that may be several meters deep. The most part of regolith is composed of particles of the size of dust. The primary component of lunar regolith is dust, which poses a serious risk since it may get embedded in devices like computers, rover sensors, and systems for human protection and survival. Currently, many researchers are attempting to comprehend the characteristics of lunar dust, the consequences of human exposure, and strategies to reduce its harmful impacts [3, 4].

Along with Mercury, Venus, and Earth, Mars is the fourth and last terrestrial planet in the solar system. It is distinguished by a solid surface that has been impacted by meteorites and climatic change [5, 6]. Mars seasons follow a similar cycle to Earth ones due to the planet tilt present in its rotation axis, but with more variations in temperature and season duration [7–11]. Mars does not have an active magnetic field; the southern hemisphere nevertheless contains residual magnetism [12]. Summertime temperatures in latitudes of 60° vary from 180 to 290 K, whereas near the equator they range from 210 to 220 K. At the poles, wintertime temperatures fall below 150 K [13]. At the base of the Hellas Basin, the absolute pressure of the environment is 14 mbar, whereas at the greatest height, it is 3 mbar [11, 13]. Organic matter decomposes quickly in the absence of ozone because brief UV light reaches the soil [13].

A habitat modulus on a mobile space exploration and colonization spacecraft is described in this study [14, 15]. The mobility vehicle has two compass legs that hold up the habitat modulus. A system of ropes coiled on pulleys controls the height of the habitat modulus, the trim during motion, and lowering and climbing. Because of their advantageous high strength/mass ratio, flexibles are frequently used in aeronautical systems [16, 17]. The pulley system that makes up the open ring control has a changeable radius. With the compass legs sitting on the ground and functioning like legs with a controlled movement at the base, the vehicle may travel forward or backward [18].

2 Vehicle-habitat

2.1 The trim control strategy

The goal of the intrinsic control system is to maintain constant the height of the habitation module with

respect to the ground, during the motion of the vehicle. The latter advances with an opening and closing motion of the legs of the compasses, which constitute the mobile support structure of the habitation module. The intrinsic control system of the quota is made up of a mechanism that uses flexible ropes that wind around pulleys. Figure 1 schematically represents the forward motion of the vehicle.

Considering the vehicle geometry, two symmetry planes can be found. There are both a longitudinal symmetry plane π1, in which the motion of the centre of the system lies, and a transversal symmetry plane π2, containing the axis of the top hinge. Both planes π1 and π2 are perpendicular to the ground plane, as seen in Fig. 2.

Due to these symmetries, in order to represent the entire vehicle motion, it is possible to observe only one leg of one of the two compasses. This motion is representative of the motion of the entire vehicle.

It is intended to keep the height ***H*** of the habitation module constant, with respect to the ground. Referring to Fig. 3, an advancing phase is considered: the compass changes its angle β, because of the foot A advances and the foot D' is stopped on the ground. The next step will have foot A stopped and foot D' moving forward.

In Fig. 3, above, it can be seen a detail of the gear train at the top of the compass. Both the right leg 2 and the pulley linked to it are shown, while the flexible rope and left leg 1 are shown on the left.

Each leg is connected to a pulley on which a rope is wound; the free end of the rope is connected to the cart that slides on the other leg. In Fig. 3, above, legs 1 and 2 of one of the compasses and one of the two pulleys are shown, the other pulley is omitted for the clarity of the drawing; the represented pulley is the one attached to the right leg 2, on which it is wrapped around a rope with the free end connected to the trolley which slides on the left leg 1. One of the two sides of the transversal beam 3, carrying the habitation module, is supported by this cart. The same happens for the other leg of the compass: on the other side the situation is symmetrical. Looking again at Fig. 3, on the right, it can be seen the leg AB, of one of the two compasses, when A advances to A'. The other leg, however, has the foot still on the ground. During the advancement, the inclination φ of the leg, with respect to the ground, changes; in the same way the inclination of the other leg BD of the compass, which has the stationary foot, changes symmetrically.

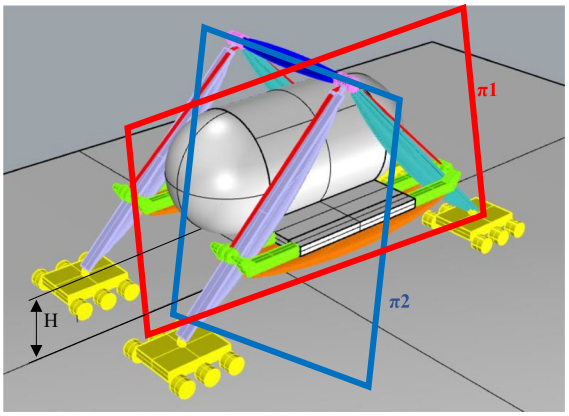

Fig. 2 The complete vehicle and the symmetry planes π1 and π2

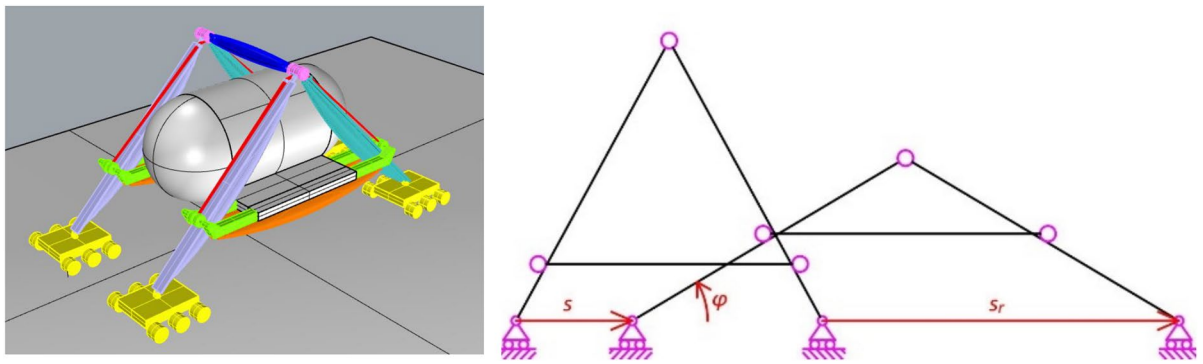

Fig. 1 The vehicle and the advancing strategy

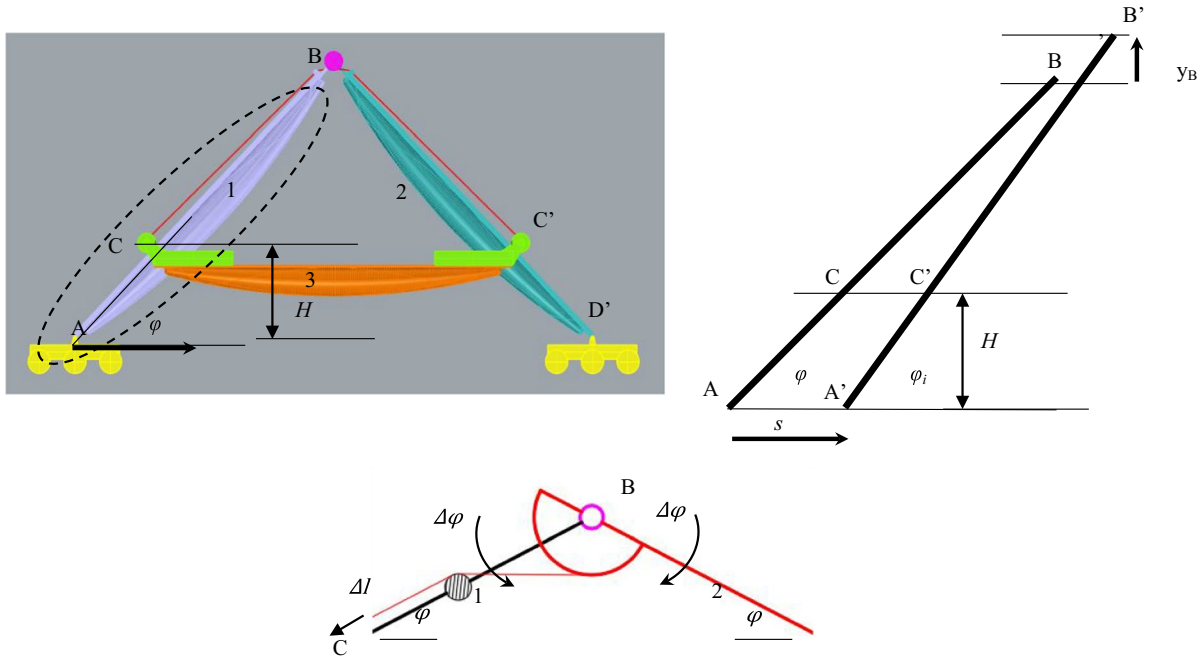

Fig. 3 A leg of one of the compasses is representative of the motion of the entire vehicle

The length of the leg, in Fig. 3, corresponds to the length of the segment AB, since the leg is considered to have a straight axis. The height H from the ground of the habitation module is required to be kept constant. The length of the segment BC increases as the angle φ_i increases when the foot A of the leg advances in A′, while the length A′C′ decreases respect to AC.

A rope connects the top of the leg, point B, to point C where there is the connection point between the axis of the leg and the habitation module.

Considering a generic angle φ_i, during the forward motion of the foot A of the leg, it is possible to write the expression of the variation ΔL of the rope connecting points B and C.

$$\begin{aligned} &\Delta L = B'C' - BC; BC = AB - AC; B'C' = A'B' - A'C'; AB = A'B' \\ &\Delta L = B'C' - BC = \left(A'B' - A'C'\right) - (AB - AC) = AC - A'C' \end{aligned} \tag{1}$$

$$AC = \frac{H}{sen(\varphi)}; A'C' = \frac{H}{sen\left(\varphi_i\right)} \tag{2}$$

$$\Delta L = \frac{H}{sen(\varphi)} - \frac{H}{sen\left(\varphi_i\right)} = H\frac{sen\left(\varphi_i\right) - sen(\varphi)}{sen(\varphi) \cdot sen\left(\varphi_i\right)} \tag{3}$$

Figure 4 shows the variation of the length of the flexible hose ΔL as the angle φ_v varies, dimensionless with respect to the total length L of the leg.

The radar diagram in Fig. 5 shows the trend of the relationship between the radius R of the pulley on which the flexible winds and unwinds during the motion of the vehicle to maintain the habitation module height constant. This quantity is referred dimensionless with respect to the length of the compass leg. R/L in Fig. 5 is shown vs the angle $\vartheta = 2\varphi$. Referring to Fig. 3, the angle $\vartheta = 2\varphi$ is the angle by which the pulley, which is bound to leg 2, BD', rotates with respect to leg AB, therefore it is the angle of winding and unwinding of the flexible during the motion of the legs, to keep the height H constant of the

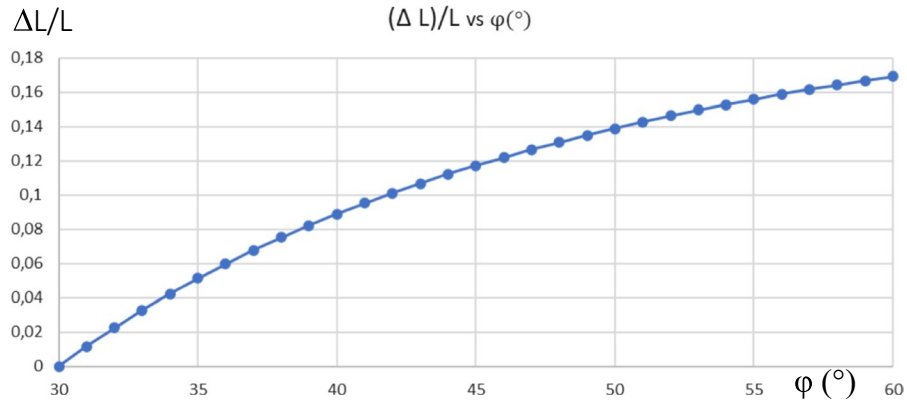

Fig. 4 Dimensionless trend of the variation of the length of the hose vs angle β

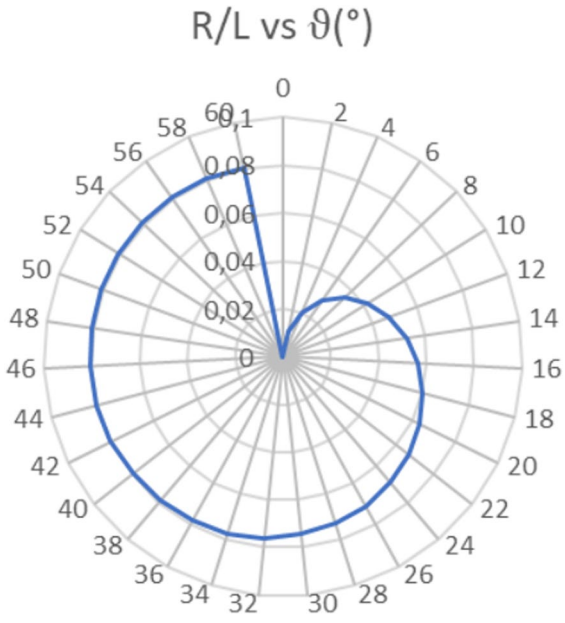

Fig. 5 R/L angular profile of the pulley radius to obtain a constant quota of the habitation module equal to one fifth of the length of the leg

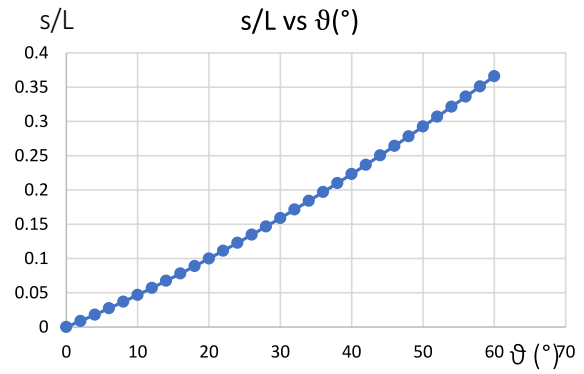

Fig. 6 The advancement s vs the angle ϑ between the two legs of the compass

habitation module. This diagram represents the profile of the pulley to obtain the required performance which consists in maintaining the constant height H of the habitation module, with respect to the ground, as the legs move.

The case represented refers to a ratio between the height of the habitation module from the ground and the length of the leg of 1/5. For different ratios the calculation follows the same steps.

For a more complete representation of the motion, the advancement s of the leg foot is shown, in Fig. 6, dimensionless with respect to the length L of the leg vs the variation in the angle ϑ between the two legs of the compass.

Figure 7 shows, depending on the advancement of the foot, the advancement of the midpoint of the habitation module and the variation of the position in height of the vertex of the compass vs the advancement of the foot s. These quantities are all shown dimensionally with respect to the length L of the compass leg.

2.2 The equilibrium

To examine the compass mechanism, consider the simplified diagram in Fig. 8. The structure is examined when the following variables vary, the rods are taken to be rigid bodies, and the masses are supposed to be concentrated at each rod center of gravity.

The parameters changing during the motion are:

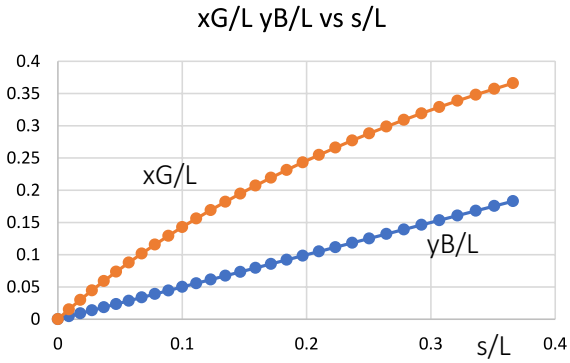

Fig. 7 The advancement of the midpoint of the habitation module and the variation of the position in height of the vertex of the compass vs the advancement of the foot s

φ Angle at the base of the rods;

φ_0 Angle in the initial configuration of the rising phase;

φ_1 Angle in the final configuration of the ascent phase, coincident with the angle of the initial configuration of the opening phase at constant height;

$\varphi 2$ Angle of the final configuration of the opening phase at constant altitude;

m_1 Mass of rod 1;

m_2 Mass of rod 2;

m_3 Mass of rod 3 (middle rod)

La = L Length of the side rods, assuming they have the same length;

d_1 Distance of the center of mass of rod 1 from the end resting on the ground;

d_2 Distance of the center of mass of rod 2 from the end resting on the ground;

d_3 Distance of the center of mass of rod 3 from the left end;

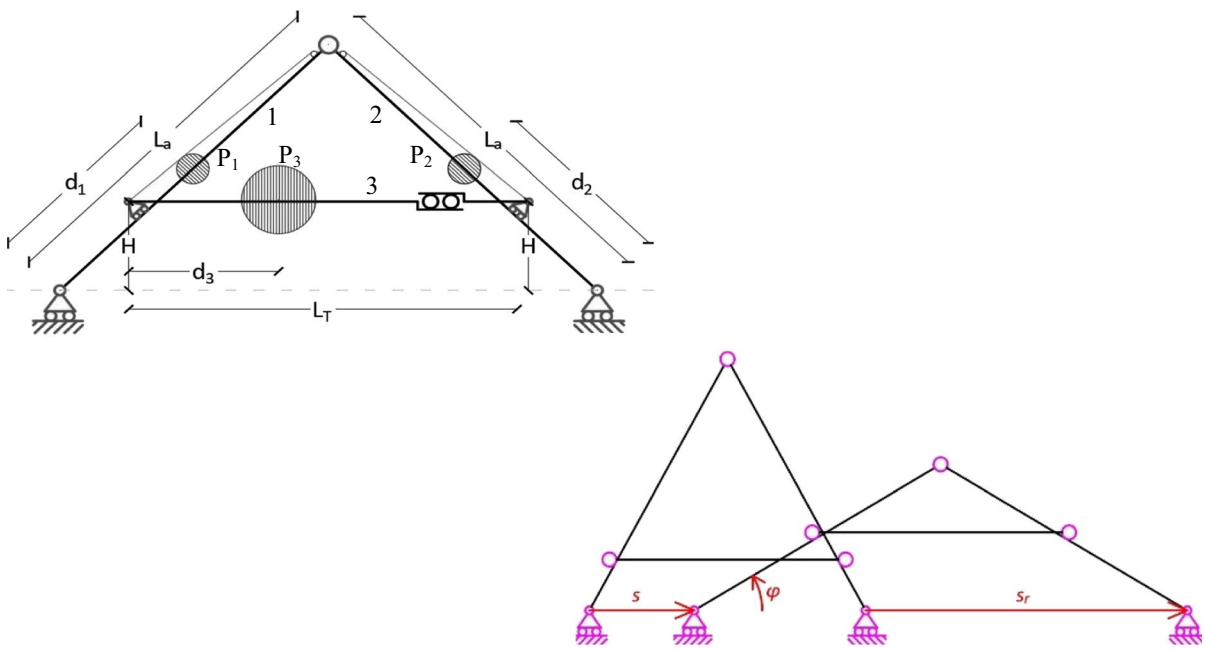

Fig. 8 Compass mechanism scheme displaying the primary geometric characteristics that define the structure. The habitat to the center rod and the material point comparable to the mass of the side rods are shown by the circles

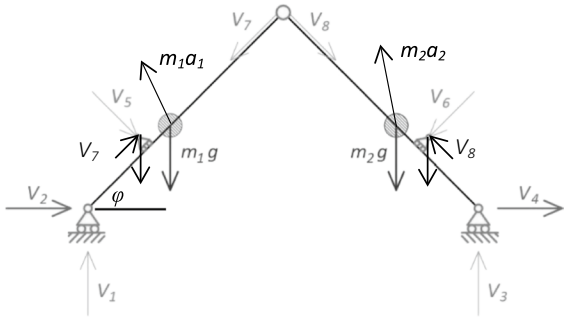

Fig. 9 Diagram showing the forces acting on lateral beams and their self-weight

L_T Distance between the two constraints of rod 3 (center), it differs from the length of this rod in that L_T varies with the angle;

H Elevation with respect to the ground of rod 3 (center);

s Displacement imposed at the base of the left constraint;

s_r Displacement of the right-hand constraint.

The center rod and the side rod assembly make up the two components of the compass mechanism. The lateral rod assembly interacts with the ground through two constraints. These constraints act as hinges in a static situation, act as hinge and roller support when one support moves and the other is fixed, or both act as roller supports when both constraints move.

Furthermore, the center rod exhibits a support-barrel-like pattern where the beam length varies based on the opening and shut-ting of the compass mechanism. The general dynamic model is described, where the three material points have non-negligible accelerations. The body overall dynamic equilibrium equations in the X and Y axes are written, referring to the free body diagram shown in Fig. 9:

$$V_2 + V_4 - m_1a_{1x} - m_2a_{2x} - m_3a_{3x} = 0 \tag{4}$$

$$V_1 + V_3 - (m_1 + m_2 + m_3)g - m_1a_{1y} - m_2a_{2y} - m_3a_{3y} = 0 \tag{5}$$

The equation relating V_6 and V_8 can be expressed in such a way that the restraint is considered as a roller support that allows free movement along the axis of the legs. The same can be done for the equation linking V_5 and V_7.

$$V_8 = V_6\tan\varphi \tag{6}$$

$$V_7 = V_5\tan\varphi \tag{7}$$

The dynamic equilibrium equations for rod 3 (the center rod), as in in Fig. 8, may be written in the X and Y directions as well as at rotation around the left end:

$$-V_5\sin\varphi + V_7\cos\varphi - m_3a_{3x} = 0 \tag{8}$$

$$V_5\cos\varphi + V_7\sin\varphi + V_6\cos\varphi + V_8\sin\varphi - m_3a_{3y} - m_3g = 0 \tag{9}$$

$$(V_6\cos\varphi + V_8\sin\varphi)L_T - (m_3a_{3y} + m_3g)d_3 = 0 \tag{10}$$

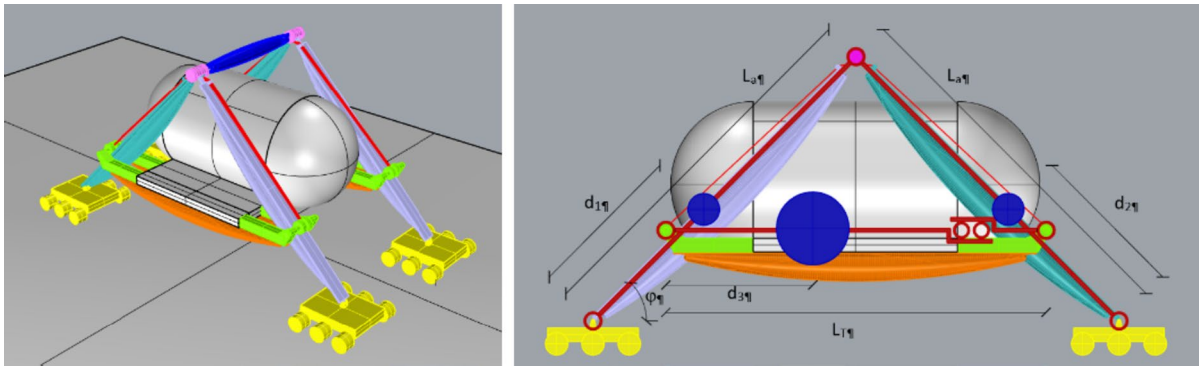

Fig. 10 The vehicle-with the habitat modulus and the compass structure

The equation expressing the rotating equilibrium of the rod 1 (Figs. 8 and 9), with respect to the vertex of the compass, in the anticlockwise direction, is:

$$\begin{aligned} &- V_1 L_a \cos\varphi \; + \; V_2 L_a \sin\varphi + V_5\left(L_a - \frac{H}{\sin\varphi}\right) \\ &+ \left(m_1 a_{1y} + m_1 g\right)\left(L_a - d_1\right)\cos\varphi + \\ &- m_1 a_{1x}\left(L_a - d_1\right)\sin\varphi = 0 \end{aligned} \tag{11}$$

The equation expressing the rotating equilibrium of the rod 1 (Figs. 8 and 9), with respect to the vertex of the compass, in the anticlockwise direction, is:

$$\begin{aligned} &V_3 L_a \cos\varphi + \; V_4 L_a \sin\varphi - V_6\left(L_a - \frac{H}{\sin\varphi}\right) \\ &- \left(m_2 a_{2y} + m_2 g\right)\left(L_a - d_2\right)\cos\varphi + \\ &- m_2 a_{2x}\left(L_a - d_2\right)\sin\varphi = 0 \end{aligned} \tag{12}$$

Furthermore, L_T is defined as:

$$L_T = 2\cos\varphi\left(L_a - \frac{H}{\sin\varphi}\right) \tag{13}$$

With quasi-stationary motion, V_2 and V_4 both take on the role of constraining forces, but when it comes to dynamic motion, they alternately take on the role of constraining force and external action.

Elaborating the previous equations, a system of two equations in the unknowns V_2, V_4, and s is obtained. It will be necessary to make at least two additional assumptions regarding the previous unknowns to solve the problem. These assumptions could be quasi-stationary motion, which ignores inertial forces and displacement s, or imposed motion, which uses the function of displacement s and angle φ, as shown in Fig. 8.

$$V_2 + V_4 - m_1 a_{1x} - m_2 a_{2x} - m_3 a_{3x} = 0 \tag{14}$$

$$\begin{aligned} &\left(V_4 - V_2\right) + m_3 a_{3x}\left(1 - \frac{H}{L_a \sin\varphi}\right) + \left(m_3 a_{3y} + m_3 g\right)\frac{H\cos\varphi}{L_a \sin^2\varphi} \\ &+ \frac{\left(m_1 a_{1y} + m_1 g\right)}{\tan\varphi}\frac{d_1}{L_a} + \frac{\left(m_2 a_{2y} + m_2 g\right)}{\tan\varphi}\frac{d_2}{L_a} + m_1 a_{1x}\left(1 - \frac{d_1}{L_a}\right) - m_2 a_{2x}\left(1 - \frac{d_2}{L_a}\right) = 0 \end{aligned} \tag{15}$$

Once the values of the two forces, V_2 or V_4, are known, Eqs. (14) and (15) allow the motion of the compass to be calculated. The hourly law of the force, to ensure motion in the event of an assumed motion, may be found by simply deriving the hourly law of the assumed motion and reinserting it into the formulae expressing V2 and V4 (see Fig. 10).

If there are no dissipative processes and there are only rigid bodies, the total mechanical energy $\boldsymbol{E}$ may be expressed as follows:

$$\begin{aligned} E = U + K = &\sin\varphi\left(m_1 g d_1 + m_2 g d_2 + m_3 g H\right) + m_1 g d_1 \\ &+ \frac{1}{2}m_1\left(v_{1x}^2 + v_{1y}^2\right) + \frac{1}{2}m_2\left(v_{2x}^2 + v_{2y}^2\right) + \frac{1}{2}m_3\left(v_{3x}^2 + v_{3y}^2\right) \end{aligned} \tag{16}$$

In Eq. (16), $\boldsymbol{U}$ represents the gravitational potential energy and $\boldsymbol{K}$ is the kinetic energy. The work of the external forces is equal to the variation of the mechanical energy $\boldsymbol{E}$.

Referring to Fig. 8, the three material points P_1, P_2 and P_3, associated with the rods, have acceleration obtained from the derivative of their positions; the rods masses are concentrated in the center of gravity. The positions of the three material points P_1, P_2 and P_3, associated with the rods, are expressed below, supposing that the central rod remains horizontal, assuming, in general, that the height H from the ground of the central rod can vary in time and assuming, furthermore, that the sliding constraint in the lower left corner of the compass moves by a displacement $\boldsymbol{s(t)}$:

$$\begin{aligned} P_1 &= \left(d_1\cos\varphi + s; d_1\sin\varphi\right) \\ P_2 &= \left(\left(2L_a - d_2\right)\cos\varphi + s; d_2\sin\varphi\right) \\ P_3 &= \left(H\cot\varphi + d_1\cos\varphi + s; H\right) \end{aligned} \tag{17}$$

The velocities and the accelerations of the center of mass of the rods 1, 2 and 3 are expressed, deriving in time, as follows.

$$
\begin{aligned}
v_1 &= \left(-\dot{\varphi} d_1 \sin\varphi + \dot{s}; \dot{\varphi} d_1 \cos\varphi\right) \\
v_2 &= \left(-\dot{\varphi}\left(2L_a - d_2\right)\sin\varphi + \dot{s}; \dot{\varphi} d_2 \cos\varphi\right) \\
v_3 &= \left(-\frac{H\dot{\varphi}}{\sin^2\varphi} + \dot{H}\cot\varphi + \dot{s} - d_1 \sin\varphi; \dot{H}\right)
\end{aligned} \tag{18}
$$

The previous equations are conditions to be satisfied for the function $H(\varphi)$ and the values $H(\varphi_0) = H_0$ and $H(\varphi_1) = H_1$ must be reached. A parabolical function with a vertex at φ_1 is a function that satisfies these conditions:

$$
\begin{aligned}
a_1 &= \left(d_1\left(-\ddot{\varphi}\sin\varphi - \dot{\varphi}^2\cos\varphi\right) + \ddot{s}; d_1\left(\ddot{\varphi}\cos\varphi - \dot{\varphi}^2\sin\varphi\right)\right) \\
a_2 &= \left(\left(2L_a - d_2\right)\left(-\ddot{\varphi}\sin\varphi - \dot{\varphi}^2\cos\varphi\right) + \ddot{s}; d_2\left(\ddot{\varphi}\cos\varphi - \dot{\varphi}^2\sin\varphi\right)\right) \\
a_3 &= \left(\frac{H}{\sin^2\varphi}\left(-\ddot{\varphi} + 2\dot{\varphi}^2\cot\varphi\right) + \ddot{H}\cot\varphi + \ddot{s} - d_1\dot{\varphi}^2\cos\varphi - d_1\ddot{\varphi}\sin\varphi; \ddot{H}\right)
\end{aligned} \tag{19}
$$

The inertial forces, acting on the compass system are negligible in quasi-stationary motion. Assuming zero acceleration values the quasi-stationary motion is described by the generic Eqs. (4) and (14).

2.3 Vehicle ascent mode

Prior to analyzing this mode, the function H(t) must be defined. This function must assume that, at the extremes of the rising mode time interval, $H(t_0)=H_0$ and $H(t_1)=H_1$. Since the rod (3) must stop when it reaches the height, it must be taken into consideration that the velocities of the compass centers of mass are zero at the starting moment, $t=t_0$, and at the final instant, $t=t_1$. Under these circumstances, the following values are obtained for the velocity of the centers of mass in rods 1 (left), 2 (right), and 3 (middle): at the beginning instant $t=t_0$, at the end instant $t=t_1$. A step movement is analyzed, where it is possible to consider $s=0$. To impose null the velocities of the compass rods 1 and 2 for $t=t_0$ and $t=t_1$, it is enough that:

$$
\dot{\varphi}(t_0) = \dot{\varphi}(t_1) = 0 \tag{20}
$$

To impose null the velocity of the rod 3, it is necessary that $\dot{H}=0$

$$
\dot{H} = \frac{dH}{d\varphi}\dot{\varphi} = H'\dot{\varphi} \tag{21}
$$

At the beginning instant $t=t_0$ and the ending instant $t=t_1$, condition (18) must also be respected.

$$
H'(\varphi_1) = 0 \tag{22}
$$

$$
H''(\varphi_1) = 0 \tag{23}
$$

$$
H(\varphi) = \frac{H_0 - H_1}{\left(\varphi_0 - \varphi_1\right)^3}\left(\varphi - \varphi_1\right)^3 + H_1 \tag{24}
$$

3 Conclusions

This work describes and analyzes a habitat vehicle which is required, in terms of performance, to be able to carry out a forward motion while maintaining constant the height of the habitat modulus and, furthermore, it is required to be able to carry out loading and discharge to the ground. The analyzes of the habitat vehicle behavior, with the models defined, even if within the hypotheses, have highlighted how the performances are achievable with the proposed vehicle scheme. As such, the authors consider these models to be a useful reference for the habitation module design.

Future developments will focus on studying the behavior of the vehicle when the motion is outside the vertical plane of symmetry, the plane in which the models in this work are defined. Furthermore, a fundamental theme of the development of the work will concern friction both in the mechanisms of the residential vehicle, which allow its motion, and the sliding and rolling friction at the interface with the ground.

Finally, the authors consider the study of the motorized implementation of the motion of the pulleys, on which the ropes are wound, as a future development. During descent to the ground and ascent to a defined height of the transversal beam, the pulleys impose the position of the cart along the compass beams, that are the legs of the system.

Acknowledgements This paper is part of the project NODES which has received funding from the MUR –M4C2 1.5 of PNRR with grant agreement no. ECS00000036.

Author contributions All authors have contributed equally to this work.

Funding Open access funding provided by Politecnico di Torino within the CRUI-CARE Agreement.

Data availability No datasets were generated or analysed during the current study.

Declarations

Conflict of interest The authors declare no competing interests.

References

1. Verne J (1868) De la Terre à la Lune - Trajet Direct en 97 Heures et 20 Minutes. Bibliotheque d'education e de récréation J Hetzel, Paris
2. Sokolskij VN (2004) The life and work of Konstantin E. Tsiolkovsky. Selected Works of Konstantin E. University Press of the Pacific Press, Tsiolkovsky
3. Schmitt HH, Heiken G, Vaniman D, French BM (1991) Lunar sourcebook. Cambridge University Press Cambridge, USA
4. Neal and Pieters et al (2020) Earth-moon environment. https://assets.pubpub.org/krxijd00/71617915834660.pdf
5. Cohen MM (2003) Mobile lunar and planetary bases. AIAA, Reston, Virginia, USA
6. Seedhouse E (2015) Bigelow aerospace: colonizing space one module at a time. Springer International Publishing, Cham
7. Ciardullo C, Yashar M, Montes J (2016) Martian ice habitats: approaches to additive manufacturing with H_2O beyond mars ice house, researchgate. AIAA, Reston, Virginia, USA
8. Yashar M, Ciardullo C (2019) Mars X-house: design principles for an autonomously 3D- printed ISRU surface habitat, researchgate, In: 49th international conference on environmental systems ICES-2019–268 7–11 July 2019, Boston, Massachusetts, USA
9. Weissman PR (2014) The Solar System and Its Place in the Galaxy. Encyclopedia of the solar system. Elsevier, Amsterdam, The Netherlands
10. Buis A (2020) Milankovitch (Orbital) Cycles and their role in earth's climate. NASA's Jet Propulsion Laboratory. https://climate.nasa.gov/news/2948/milankovitch-orbital-cycles-and-their-role-in-earths-climate/.
11. Barlow N (2008) Mars: an introduction to its inferior, superior and atmosphere, Chapter 6 - Atmospheric conditions and evolution. Cambridge University Press, Cambridge, UK
12. Catling DC (2014) Encyclopedia of the solar system, chapter 16 - mars atmosphere: history and surface interactions. Elsevier
13. Carr MH, Bell JF (2014) Mars: surface and interior, in encyclopedia of the solar system. Elsevier, Amsterdam, The Netherlands
14. Drake BG (2009) Human exploration of mars–design reference architecture 5.0, Mars architecture steering group. NASA document. NASA Technical report, SP-2009–566, July 2009. 15, 17, 21, 23, 113, 114, 116, 125, 145G
15. Salotti JM (2012) Revised scenario for human missions to Mars. Acta Astronaut 81(1):273–287
16. Khanakornsuksan C, Wongratanaphisan T (2020) Optimal design of a suspended cable driven system for locomotion device. Int J Mech Control 21(2):63–71
17. Inel F, Carbone G, Ceccarelli M (2020) Design and implementation of high-level control modes for a 3D cable-driven-parallel robot. Int J Mech Control 21(2):87–94
18. Bonafede G, Manuello Bertetto A, Fiorini P, Muscolo GG (2022) Compliant legs in biped robots for running optimization. Int J Mech Control 23(2):53–60